



CHALMERS
UNIVERSITY OF TECHNOLOGY

Nitridation of Three Austenitic Alloys at 1100 °C

Downloaded from: <https://research.chalmers.se>, 2025-04-06 09:57 UTC

Citation for the original published paper (version of record):

Sand, T., Rajagopal, A., Sattari, M. et al (2025). Nitridation of Three Austenitic Alloys at 1100 °C. High Temperature Corrosion of Materials, 102(2). <http://dx.doi.org/10.1007/s11085-025-10331-9>

N.B. When citing this work, cite the original published paper.



Nitridation of Three Austenitic Alloys at 1100 °C

T. Sand¹ · A. Rajagopal² · M. Sattari³ · S. Bigdeli⁴ · M. Hättestrand² ·
J.-E. Svensson¹ · M. Halvarsson³ · L.-G. Johansson¹

Received: 30 October 2024 / Revised: 27 February 2025 / Accepted: 28 February 2025
© The Author(s) 2025

Abstract

The nitridation of three austenitic high-temperature alloys in 95% N₂+5% H₂ environment at 1100 °C was evaluated in terms of gravimetry and investigated by SEM–EDS, EPMA and STEM. Samples made from Alloy 600, 253 MA and 353 MA were exposed for 1 day, 1 week and 3 weeks. Alloy 600 underwent very little nitridation, while 253 MA and especially 353 MA, were heavily affected by nitride precipitation. The nitridation of all three alloys had reached equilibrium after three weeks; the extent of nitridation depending on the chromium activity in the alloy. The kinetics of nitrogen ingress into the alloy depends on nickel concentration, while the rate-determining step in the nitridation process is the nucleation and growth of the nitride precipitates.

Keywords Alloy · SEM · EPMA · STEM · High-temperature corrosion

Introduction

To avoid formation of oxide scales on components, heat treatment operations are commonly carried out at low oxygen activity, typically using mixtures of N₂ and H₂. Such environments can cause degradation of alloys used in heat treatment furnaces by nitridation, limiting the life of the process equipment. The dissolution of nitrogen into the alloy results in a deterioration of properties, the formation of nitride precipitates being particularly harmful. Thus, nitrogen which dissolves into Cr-containing

✉ T. Sand
tommy.sand@chalmers.se

¹ Department of Chemistry and Chemical Engineering, Chalmers University of Technology, S-412 96 Gothenburg, Sweden

² Alleima, S-811 81 Sandviken, Sweden

³ Department of Physics, Chalmers University of Technology, S-412 96 Gothenburg, Sweden

⁴ Höganäs AB, S-263 39 Höganäs, Sweden

alloys at high temperature can form chromium nitride precipitates in the alloy bulk, causing embrittlement and chromium depletion of the alloy matrix.

The ability of an alloy to resist nitridation relies both on the intrinsic properties of the alloy and on its ability to form an oxide scale which can act as a barrier toward nitrogen uptake. It was recently reported that while the presence of a chromia scale reduced the nitridation rate of five austenitic high-temperature alloys by 50–95% at 900 °C. Indeed, a defect-free alumina scale formed on ferritic FeCrAl alloys appeared to be impermeable to nitrogen under the same conditions [1].

In the absence of a surface oxide, the ability to resist nitridation primarily depends on alloy chemistry. Thus, the tendency to suffer nitridation increases with the concentration of chromium and other nitride formers, such as aluminum and titanium, in the alloy [2, 3]. Aluminum and titanium have higher affinity for nitrogen than chromium and the corresponding nitrides tend to precipitate prior to chromium nitride [4]. Since most high-temperature alloys contain relatively high concentrations of chromium to provide protection against oxidation and other types of corrosion, nitridation can become a serious issue.

The rate of nitridation can be limited either by the uptake of nitrogen at the alloy surface or by transport of dissolved nitrogen in the alloy bulk. The uptake of nitrogen by the alloy from $N_2(g)$ is preceded by adsorption and dissociation of the N_2 molecule on the alloy surface. Because of the strength of the molecular bond in N_2 , this process can be slow and rate limiting for nitridation. It is reported that N_2 dissociation on surfaces is catalyzed more readily by iron compared to nickel and the kinetics of nitrogen uptake are expected to become slower with increasing nickel content [5]. Nitrogen transport in austenitic alloys is promoted by high solubility and high diffusivity. While the solubility of nitrogen in austenite is higher than in ferrite [6], the diffusivity of nitrogen in austenite is much slower than in ferrite [7]. In addition, nitrogen solubility in austenite is reported to decrease rapidly with increasing nickel content [4, 8].

Above 1050 °C in 1 atm. N_2 , Cr_2N is the only stable chromium nitride [9, 10]. In pure chromium and in alloys with very high amounts of chromium, chromium nitride forms a continuous surface layer. In Fe- Ni- and Co-base alloys, and in temperatures relevant for this study, chromium nitride precipitates form a dispersion in the alloy [11]. Nitrogen is dissolved interstitially in the austenitic matrix, and the depth of nitridation depends on various factors, including the diffusivity of nitrogen [12].

Nitridation as corrosion has been investigated by Tjokro and Young [4] who reported on the nitridation of several commercial alloys at 1000–1200 °C in NH_3 and $N_2 + H_2$ environments, focusing on the kinetics and microstructure of nitridation. They reported that the kinetics of nitridation were parabolic, being controlled by inward nitrogen diffusion and that Cr_2N precipitates formed both at grain boundaries and within the alloy grains. Barnes and Lai [8] compared the nitridation behavior of Fe-, Ni- and Co-base alloys in pure N_2 at 1093 °C. The exposure times were longer than in [4], and some of the samples were fully nitrided at the end of the exposures. Both [4] and [8] report that the ability of the alloys to resist nitridation showed a positive correlation with the Ni-concentration. There is also extensive literature concerning on-purpose nitriding [13–15].

The present study investigates the nitridation of three commercial austenitic high-temperature alloys, in $N_2 + H_2$ at 1100 °C. The exposures lasted 24, 168 and 504 h; the nitridation reaction approached equilibrium for all samples after 504 h. The purpose of this study is both to follow nitridation as a function of time and to investigate the situation at equilibrium. To this end, we analyze the microstructure of nitridation by several techniques and study the partitioning of chromium and nitrogen between the alloy matrix and the nitride precipitates.

Experimental Procedures

Materials

Two Fe-based and one Ni-based austenitic alloy were investigated, see Table 1 for chemical compositions. Sample coupons with the dimensions $10 \times 15 \times 2$ mm were prepared. The coupon faces were ground and polished to a mirror-bright finish with 1 μ m diamond paste in the final polishing step. Coupon edges were prepared by grinding with SiC paper with 1000# mesh grit. After polishing, the coupons were cleaned using an ultrasonic bath, first in acetone and then in ethanol. Sample thickness after final preparation was 1.5 ± 0.2 mm.

Experimental Setup

High temperature exposures were performed in horizontal tube furnaces equipped with sintered alumina reactor tubes. The environment consisted of a mixture of 95% N_2 and 5% H_2 with a 10 ± 2 ppm impurity level of H_2O corresponding to a dew point of -61 ± 1 °C. The dew point was measured using a Michelle instruments S8000 high-precision chilled mirror hygrometer. The O_2 activity in the exposure (1100 °C) was calculated to be $4 * 10^{-21}$ by Thermo-Calc using the SSUB6 database. To form a chromia scale on pure chromium at 1100 °C, an oxygen activity of about 10^{-19} is needed [16]. All exposures were performed with triplicate samples placed in alumina sample holders with 2 mm slits. Before exposure, the system was purged with N_2 for 24 h and during the final h with 95% N_2 and 5% H_2 . At the start of the exposure, the furnace reached the exposure temperature of 1100 °C in about 2 h. The exposures lasted for 24 h (1 day), 168 h (1 week) and 504 h (3 weeks). After exposure, the furnace was turned off, reaching room temperature after about 10 h.

Table 1 Chemical composition of the tested alloys (wt%)

Alloy	Cr	Al	C	Si	Mn	Ni	N	Fe	Other
253 MA	21.0		0.07	1.52	0.67	10.8	0.156	Bal	Ce
353 MA	25.7		0.07	1.39	1.68	34.9	0.172	Bal	Ce
Alloy 600	16.7	0.14	0.01	0.31	0.19	Bal	0.006	9.8	Ti

Chemical analysis were performed by X-ray fluorescence for all elements except for Al which was analyzed by spark optical emission spectroscopy and C, N that were analyzed by combustion method

The 95% N₂ and 5% H₂ environment was maintained during cooling. A comparison of quenched and furnace cooled specimens showed no difference in microstructure and mass gain.

After the exposures, the mass gains were measured using a Sartorius 6-decimal balance.

Analysis Methods

Cross-sectional samples were prepared by broad ion beam milling (BIB) using a Leica TIC3X™ and then analyzed by Scanning Electron Microscopy (SEM) with an FEI Quanta 200 microscope. Selected thin-foil samples were prepared by the focused ion beam (FIB) lift-out technique using an FEI Versa 3D FIB/SEM and subsequently examined by Scanning Transmission Electron Microscopy (STEM) using a Titan 80-300 TEM/STEM equipped with a Schottky field emission gun (FEG), a C_s-probe corrector and a high-angle annular dark field (HAADF) detector. In addition, chemical analysis was performed by energy-dispersive X-ray spectroscopy (EDS) using an Oxford X-sight detector.

Chemical analysis on the bulk samples was performed by electron probe microanalysis (EPMA) using a JEOL 8530 F-Plus equipped with five wavelength-dispersive X-ray spectrometers (WDS). The measurements were performed at an accelerating voltage of 15 kV with a current of 20 nA. The concentration profiles were measured on cross sections prepared by conventional preparation, i.e., hot embedding, grinding and polishing.

Results

Figure 1 presents mass change as a function of exposure time in the nitriding environment. Considering the evidence for internal nitridation and the lack of evidence for oxide on the sample surface (except for a thin alumina scale which formed on Alloy 600 after 3 weeks), the mass gains are attributed to the uptake of nitrogen. Indeed, the alloys investigated have been reported to form Cr₂N precipitates under similar exposure conditions [4]. All three alloys gained mass at a decelerating rate. For alloys 600 and 253 MA, there was no increase in mass between 1 and 3 weeks indicating that nitridation is completed already after 1 week. In contrast, 353 MA showed a mass gain between 1 and 3 weeks, indicating that nitridation proceeded, albeit at a slow rate. While alloy 253 MA showed the highest mass gain of the three alloys after 1 day, it is overtaken by 353 MA after 1 week. The latter alloy also showed the greatest mass gain after 3 weeks. Alloy 600 showed the lowest mass gains of the alloys studied.

Figure 2 shows cross sections of 353 MA after 1 week and 3 weeks exposure, together with EPMA line scans for chromium and nitrogen. The line scans measured the concentration of chromium and nitrogen in the alloy matrix (avoiding the nitride precipitates) across the thickness of the sample. The microstructures after 1 week and 3 weeks were similar, except that the nitride particles were slightly more

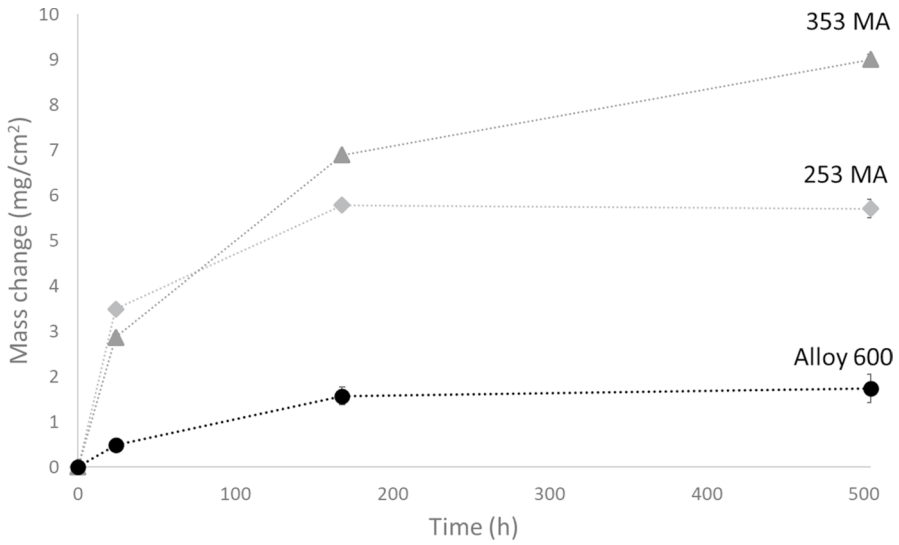


Fig. 1 Mass gain of the three alloys after exposure at 1100 °C for 1 day, 1 week and 3 weeks

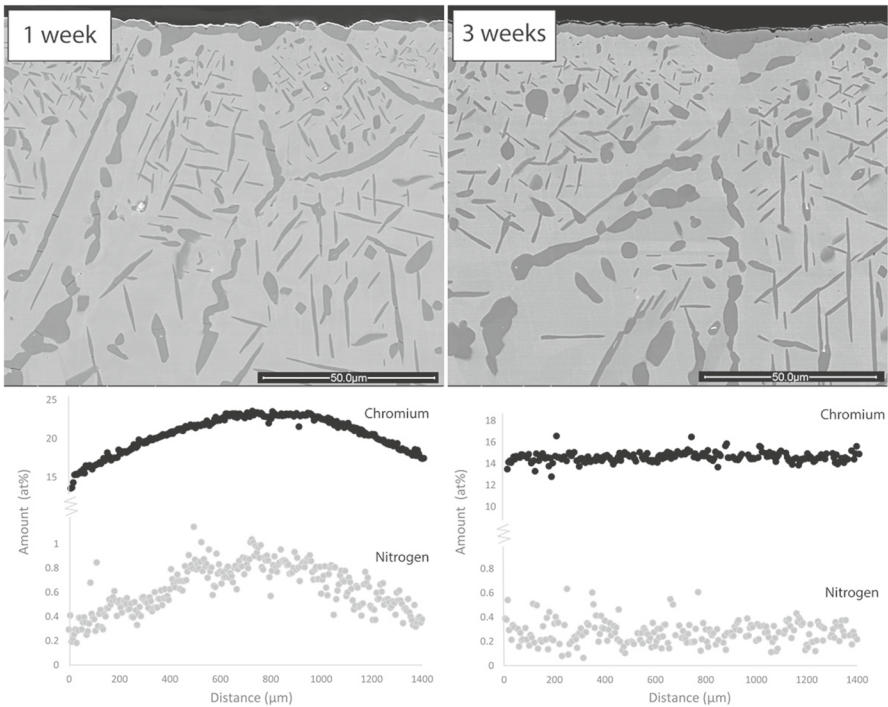


Fig. 2 SEM-BSE (backscattered electron) images showing 353 MA exposed at 1100 °C for 1 week and 3 weeks and the concentration of chromium and nitrogen in the matrix through the coupons measured by EPMA

prominent in the latter case. After 1 week, the EPMA chromium and nitrogen concentration profiles were convex, with the highest concentration of both nitrogen and chromium in the matrix occurring in the middle of the sample. In contrast, the corresponding profiles were flat after 3 weeks of exposure. At this stage, the average chromium concentration in the alloy matrix was about 14.6 at% (13.7 wt%) and the average nitrogen concentration was about 0.26 at% (0.066 wt%). The flat concentration profiles recorded after 3 weeks indicated that the nitridation process had reached equilibrium throughout the sample. At this stage, the concentrations of chromium and nitrogen in the solid solution were close to the values measured close to the surface after 1 week.

Figure 3 shows cross sections for 253 MA after 1 week and 3 weeks exposure together with EPMA line scans for chromium and nitrogen in the alloy matrix across the samples. The 1 week and 3 weeks exposures resulted in similar microstructures and nitride particle densities. In this case, the chromium and nitrogen profiles were flat already after 1 week. At this stage, the average chromium concentration in the matrix was about 17.4 at% (16.5 wt%) while the average nitrogen concentration was about 1.4 at% (0.36 wt%). These values were essentially unchanged after 3 weeks, with an average of about 17.2 at% (16.3 wt%) chromium and an average of about 1.5 at% (0.38 wt%) nitrogen. The flat chromium and nitrogen profiles after 1 week and the similarity in chromium and nitrogen concentrations after 1 week and 3 weeks

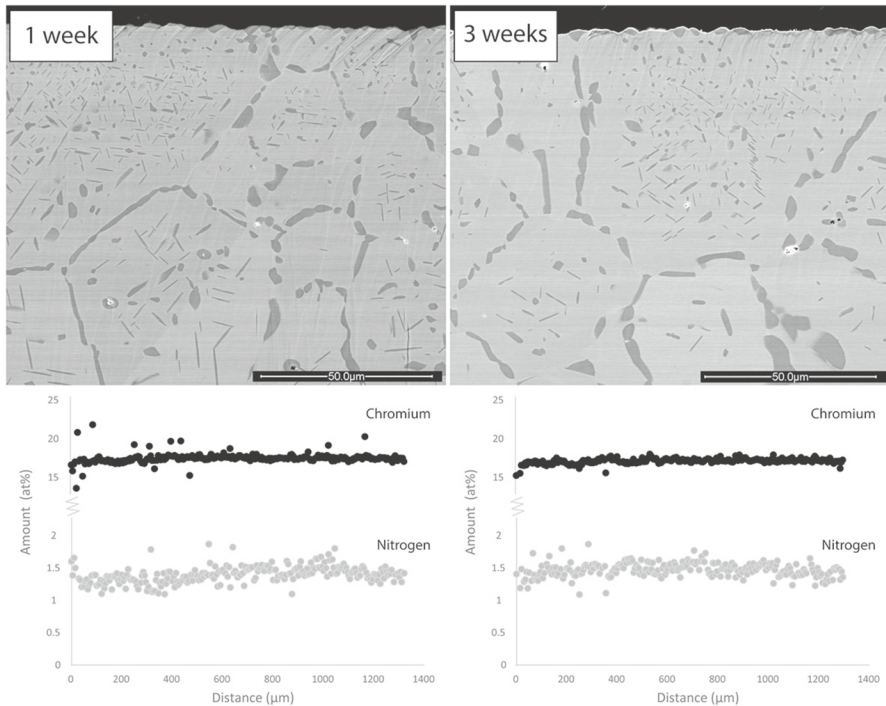


Fig. 3 SEM-BSE images showing 253 MA exposed at 1100 °C for 1 week and 3 weeks together with the concentration of chromium and nitrogen in the matrix measured by EPMA through the coupons

exposure both indicate that the nitridation of 253 MA had reached equilibrium already after 1 week.

Figure 4 shows Alloy 600 after 1 week and 3 weeks exposure together with EPMA line scans of chromium and nitrogen in the alloy matrix across the sample. The formation of precipitates in the alloy was much less pronounced compared to the two other alloys and the alloy microstructures after 1 week and 3 weeks of exposure were similar. Although the nitride particles detected in Alloy 600 were small (<500 nm), they could be avoided in the EPMA analysis of the matrix composition, see Fig. 4. After 1 week, scattered oxide particles were detected on the alloy surface. After 3 weeks exposure, an apparently continuous oxide scale had formed. The oxide scale was $1\text{--}2\ \mu\text{m}$ thick and dominated by aluminum, but also contained a significant amount of silicon, see Fig. 5. On the top surface of the oxide scale, a thin layer enriched in nickel, chromium and iron were observed. Considering the exposure conditions, it is suggested that the thin top layer is metallic. Similar to 253 MA, the chromium and nitrogen profiles were flat already after 1 week, indicating that sample nitridation had reached equilibrium. At this stage, the average concentration of chromium in the alloy matrix was about 18.4 at% (16.9 wt%) while the average nitrogen concentration was about 0.18 at% (0.045 wt%). The values recorded after 3 weeks exposure were similar, with an average of about 17.9 at% (16.5 wt%) of chromium and an average of about 0.19 at% (0.047 wt%) of nitrogen. The chromium concentration is close to the value in the unexposed alloy (see Table 1), consistent with the limited amount of nitride precipitates observed.

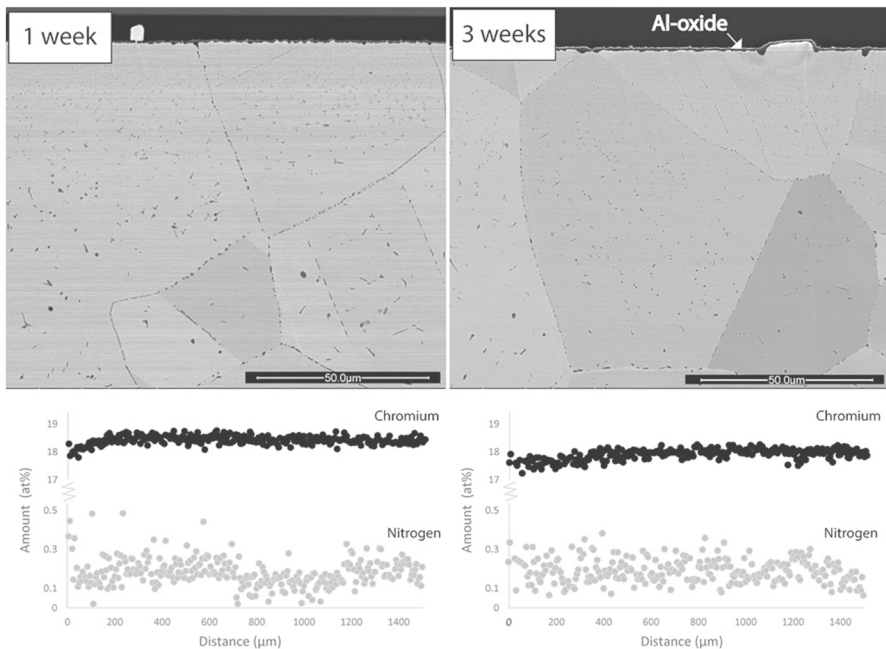


Fig. 4 SEM-BSE images showing Alloy 600 exposed at $1100\ \text{°C}$ for 1 week and 3 weeks together with the concentration of chromium and nitrogen in the matrix measured by EPMA through the coupons

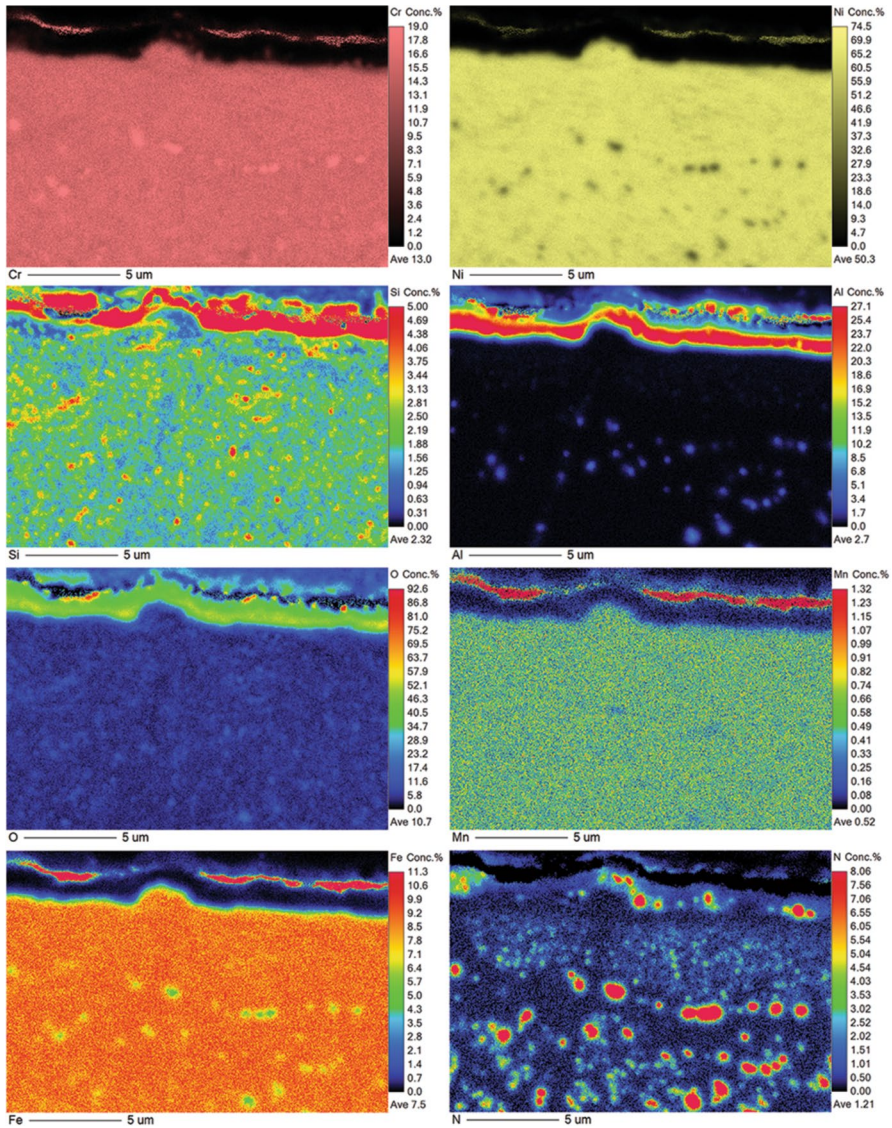


Fig. 5 EPMA-mapping of Alloy 600 exposed for 3 weeks. An external oxide scale consisting of an inner Al-rich oxide and an outer metallic layer consisting of Cr, Fe, Mn

STEM-HAADF images of 253 MA and Alloy 600 exposed for 1 week are presented in Fig. 6. The nitride precipitates in 253 MA consisted of Cr_2N containing about 10 at% iron, corresponding to the solid solution $\text{Cr}_{2-x}\text{Fe}_x\text{N}$. In Alloy 600, the nitride precipitates were considerably smaller and feature a high concentration of titanium together with chromium. By selected area electron diffraction (SAED) analysis the crystal structure was determined to be cubic, and the particles were

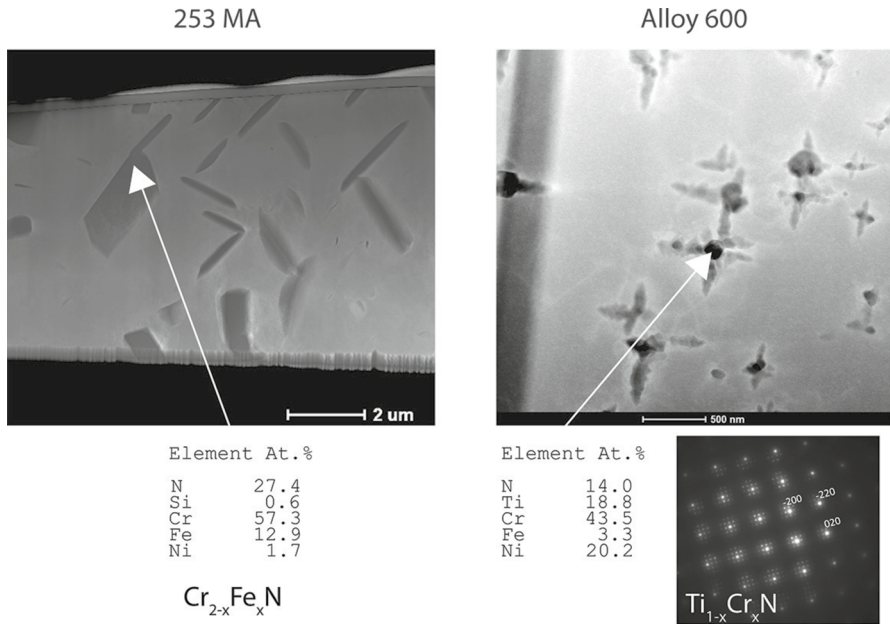


Fig. 6 STEM-HAADF images of 253 MA and Alloy 600 showing nitride precipitates after exposure for 1 week of exposure at 1100 °C. The EDS analysis shows that the nitrides in 253 MA are $Cr_{2-x}Fe_xN$. The CBED patterns together with the EDS analysis show that the precipitates in Alloy 600 are $Ti_{1-x}Cr_xN$

attributed to the halite-structured $Ti_{1-x}Cr_xN$. Because of the small size of the precipitates in Alloy 600, the elemental point analysis of the precipitates cannot avoid picking up information from the matrix, i.e., giving rise to a relatively strong nickel signal. However, after analyzing a large number of such precipitates, it was apparent that they did not contain nickel.

Discussion

All three alloys suffered nitridation during the exposures. The two alloys 253 MA and 353 MA did not show any signs of surface oxides, so all mass gain is attributed to nitrogen uptake. For Alloy 600, the uptake of oxygen due to the surface oxide after 3 weeks was calculated to account for about 18% of the total mass gain. In the cases of 253 MA and Alloy 600, the mass gain ceased after 1 week, indicating that the samples were completely nitrided (see Fig. 1). Indeed, the flat chromium and nitrogen EPMA line scans in the alloy matrix after 1 week and 3 weeks and the lack of mass gain between these measurements indicates that the nitridation reaction was essentially at equilibrium after 1 week. After 3 weeks, 353 MA also exhibited flat chromium and nitrogen profiles in the alloy matrix, implying that the nitridation reaction was close to equilibrium also in this case. In contrast, the chromium and nitrogen profiles in the 353 MA matrix were both convex after 1 week showing that the nitridation of the sample was still ongoing.

It may be noted that the nitrogen concentration in the alloy matrix in the center of the 353 MA sample was considerably higher after 1 week than after 3 weeks, implying that the alloy matrix was supersaturated with respect to Cr_2N after 1 week. This also implies that in this case, the rate-determining step in the nitridation process was the nucleation and growth of nitride precipitates rather than the uptake of nitrogen by the alloy or the transport of nitrogen into the alloy.

The composition of Alloy 600 was apparently beneficial under the experimental conditions, minimizing nitride precipitation. Because the experimental evidence indicates that the nitridation reaction was close to equilibrium at the end of the exposure, the different extent of nitride precipitation in the three alloys must be due to differences in chromium activity. Thus, the non-appearance of Cr_2N in Alloy 600 indicates a relatively low chromium activity in that alloy. This is in line with the work by Mazandarany et al. [17] who reported that in the NiCr system in the temperature range of 900–1300 °C, the activity of chromium exhibited a negative deviation from ideality (meaning $f_{\text{Cr}} < 1$). The same authors reported that additions of nickel to FeCr alloys (9–30 wt% Cr) resulted in an increased chromium activity. The latter result is in line with the observation that the concentration of chromium in the alloy matrix at the end of the exposure (at equilibrium) was lower for 353 MA than for 253 MA.

Figure 1 provides information on the kinetics of nitridation of the three alloys. Thus, 253 MA initially (24 h) exhibited faster nitridation than 353 MA, but was overtaken by the latter alloy after longer exposure times. This behavior is suggested to be explained by the lower nickel concentration in 253 MA, because the solubility and diffusivity of nitrogen in austenitic alloys are reported to decrease with increased nickel concentration [6]. Hence, the permeation of nitrogen into the alloy is expected to be faster for 253 MA. However, as nitridation approaches equilibrium, kinetic factors become unimportant, the higher chromium activity of 353 MA resulting in a higher degree of nitridation.

It is notable that Alloy 600 was able to form an apparently continuous Al-rich oxide scale after 3 weeks, despite the low aluminum content (0.14 wt%), see Fig. 5. The formation of the oxide scale is not considered to have influenced the nitridation of the alloy coupons since the nitridation reaction appears to have reached equilibrium already after one week, i.e., before a continuous alumina scale had formed on the surface. The formation of a metallic layer on top of the surface oxide on Alloy 600 in this study is in accordance with [18], where metallic Ni was reported to have diffused to the outside of the oxide scale in an environment with low oxygen activity at 950 °C.

Summary

- The nitridation of alloys 253MA and Alloy 600 in 95% N_2 + 5% H_2 environment at 1100 °C approached equilibrium after 1 week, while the reaction needed more than 1 week to be completed in the case of alloy 353 MA.

- While alloys 253 MA and 353 MA formed large amounts of hexagonal $\text{Cr}_{2-x}\text{Fe}_x\text{N}$ precipitates, Alloy 600 formed small amounts of halite-structured $\text{Ti}_{1-x}\text{Cr}_x\text{N}$ precipitates.
- The different extent of nitridation of the three alloys is attributed to the differences in chromium activity. The beneficial nitridation behavior of Alloy 600 is thus connected to its relatively low chromium activity.
- Nitridation of alloy 253 MA was initially faster than for 353 MA. This is attributed to the lower nickel content of 253 MA, which caused the transport of nitrogen into the alloy to be faster. As equilibrium was approached, kinetic factors became unimportant, the higher chromium activity of 353 MA translating into a correspondingly higher degree of nitridation.
- The rate-determining step in the nitridation of alloy 353 MA was the nucleation and growth of nitride precipitates and not the uptake of nitrogen by the alloy or the transport of nitrogen within the alloy.
- Although Alloy 600 only contains 0.14 wt% aluminum, it had formed a continuous Al-rich oxide scale after 3 weeks. However, since the oxide scale only became continuous after the nitridation reaction was completed, nitridation was not affected.

Acknowledgements This work was carried out within the Swedish High Temperature Corrosion Centre (HTC) at Chalmers University of Technology. Alleima is acknowledged for supplying materials and performing EPMA measurements.

Author Contribution TS helped in methodology, investigation, writing—original draft, visualization. AR done formal analysis. MS done formal analysis, writing—review & editing. SB helped in writing—review & editing. MH contributed to conceptualization. J-ES contributed to conceptualization, supervision, writing—review & editing. MH contributed to conceptualization, writing—review & editing. L-GJ contributed to conceptualization, supervision, writing—review & editing.

Funding Open access funding provided by Chalmers University of Technology.

Data Availability The raw/processed data required to reproduce these findings cannot be shared at this time due to technical or time limitations.

Declarations

Conflict of interest The authors declare no competing interests.

Open Access This article is licensed under a Creative Commons Attribution 4.0 International License, which permits use, sharing, adaptation, distribution and reproduction in any medium or format, as long as you give appropriate credit to the original author(s) and the source, provide a link to the Creative Commons licence, and indicate if changes were made. The images or other third party material in this article are included in the article's Creative Commons licence, unless indicated otherwise in a credit line to the material. If material is not included in the article's Creative Commons licence and your intended use is not permitted by statutory regulation or exceeds the permitted use, you will need to obtain permission directly from the copyright holder. To view a copy of this licence, visit <http://creativecommons.org/licenses/by/4.0/>.

References

1. T. Sand, et al., *Corrosion Science* **197**, 2021 (110050).
2. H. J. Christ, S. Y. Chang, and U. Krupp, *Materials and Corrosion-Werkstoffe Und Korrosion* **54**, (11), 2003 (887–894).
3. S. Y. Chang, U. Krupp, H. J. Christ, in *Cyclic Oxidation of High Temperature Materials: Mechanisms, Testing Methods, Characterisation and Life Time Estimation*, M. Schutze and W.J. Quadackers, Editors. (1999, pp. 63–81).
4. K. Tjokro and D. J. Young, *Oxidation of Metals* **44**, (3–4), 1995 (453–474).
5. C. J. H. Jacobsen, et al., *Journal of the American Chemical Society* **123**, (34), 2001 (8404–8405).
6. H. Wriedt and O. Gonzalez, *Transactions of the metallurgical society of AIME* **221**, (3), 1961 (532–535).
7. J. Fridberg, L.-E. Torndahl, and M. Hillert, *Jernkontorets Ann* **153**, (6), 1969 (263–276).
8. J. J. Barnes and G. Y. Lai, *Journal De Physique Iv* **3**, (C9), 1993 (167–174).
9. A. Soleimani-Dorcheh and M. C. Galetz, *Oxidation of Metals* **84**, (1–2), 2015 (73–90).
10. O. Kubaschewski, *International Series on Material Science and Technology* **24**, 1977 (478).
11. M. Udyavar and D. J. Young, *Corrosion Science* **42**, (5), 2000 (861–883).
12. D. L. Douglass, *JOM* **43**, (11), 1991 (74–79).
13. R. E. Schacherl and E. J. Mittemeijer, *Journal of Heat Treatment and Materials* **59**, (5), 2022 (312–319).
14. E. J. Mittemeijer and M. Somers, *Surface Engineering* **13**, (6), 1997 (483–497).
15. N. Nakada, et al., *CALPHAD-Computer Coupling of Phase Diagrams and Thermochemistry* **47**, 2014 (168–173).
16. Gleeson B, in *Shreir's Corrosion*, B. Cottis, et al., Editors. (Elsevier, Oxford, 2010, pp. 180–194).
17. F. Mazandarany and R. Pehlke, *Metallurgical Transactions* **4**, (9), 1973 (2067–2076).
18. M. Bobeth, et al., *Acta Metallurgica et Materialia* **40**, (10), 1992 (2669–2676).

Publisher's Note Springer Nature remains neutral with regard to jurisdictional claims in published maps and institutional affiliations.